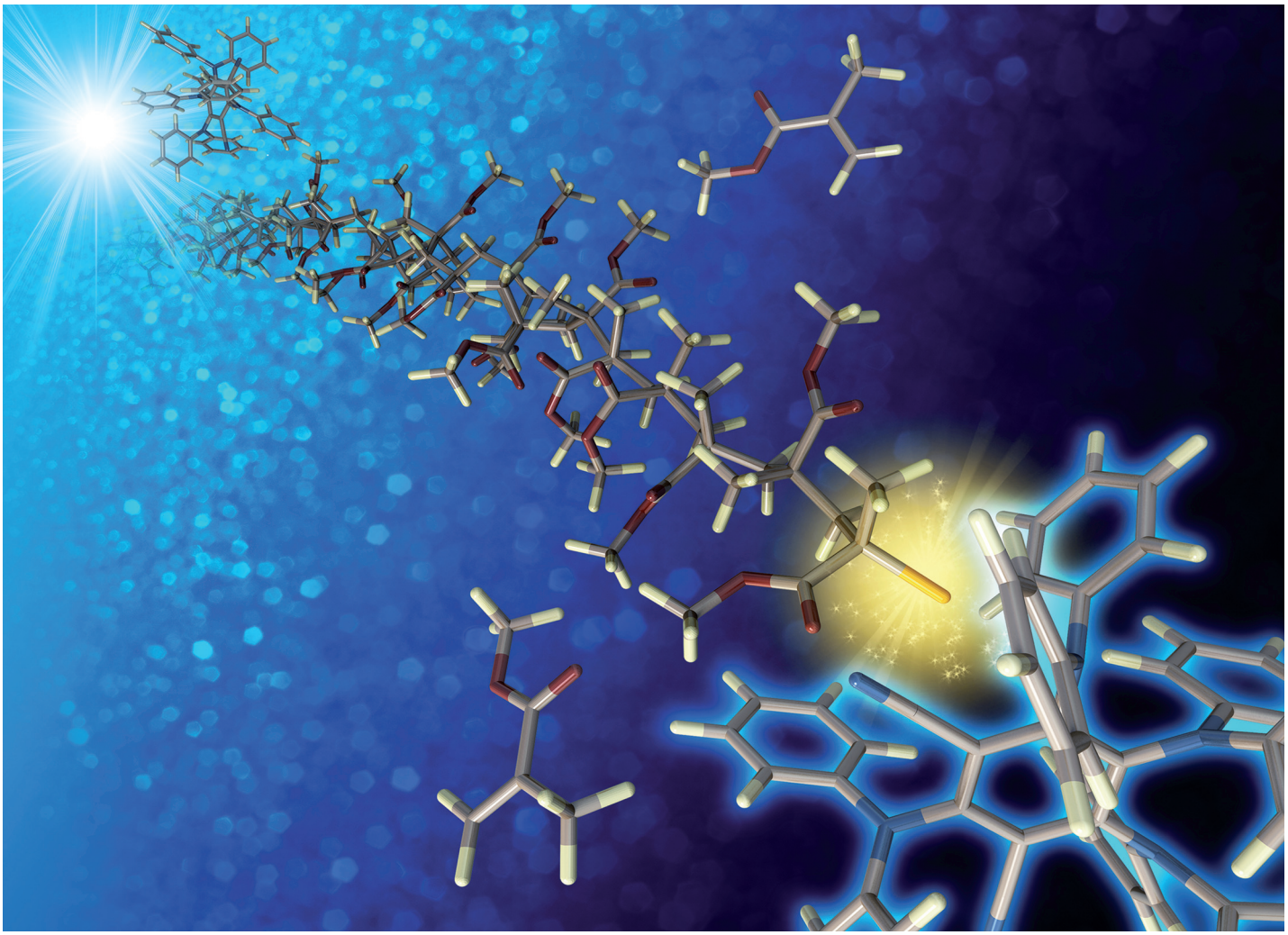

Showcasing research from Professor Kwon's laboratory, Department of Materials Science and Engineering, Seoul National University, Seoul, South Korea.

Synthesis of solvent-free acrylic pressure-sensitive adhesives *via* visible-light-driven photocatalytic radical polymerization without additives

Solvent-free acrylic PSAs were prepared through visible-light driven photocatalytic free radical polymerization. Combined experiments and quantum chemical calculations suggest that *N*-vinyl-based monomer facilitates the electron transfer between the monomer and the photocatalyst, which is responsible for the enhanced rate and conversion of polymerization. Viscoelasticity, mechanical strength and adhesion performance of acrylic PSAs were nicely adjusted in a broad range by controlling the monomer composition, suggesting that our new method would replace the existing photoinitiated free radical polymerization.

As featured in:

See Johannes Gierschner, Wonjoo Lee, Min Sang Kwon *et al.*, *Green Chem.*, 2020, **22**, 8289.

ROYAL SOCIETY OF CHEMISTRY

rsc.li/greenchem

Registered charity number: 207890

Green Chemistry

PAPER

View Article Online
View Journal | View Issue

Cite this: *Green Chem.*, 2020, **22**, 8289

Synthesis of solvent-free acrylic pressure-sensitive adhesives *via* visible-light-driven photocatalytic radical polymerization without additives†

Jong-Ho Back,[a] Yonghwan Kwon,[b,c] Juan Carlos Roldao,[d] Youngchang Yu,[a] Hyun-Joong Kim,[e] Johannes Gierschner, *[d] Wonjoo Lee*[a] and Min Sang Kwon *[b]

Research on solvent-free acrylic pressure-sensitive adhesives (PSAs) has tremendously grown over the last few decades due to the stringent regulations to control volatile organic compound emissions. They are mostly prepared in the presence of photoinitiators using high-energy UV light that causes several issues such as those associated with radiation safety. Herein, for the first time, solvent-free acrylic PSAs were prepared through visible-light-driven photocatalytic free radical polymerization. Importantly, we found that the use of *N*-vinyl-based monomers noticeably enhances the rate and conversion of polymerizations, thereby eliminating the need for additives (*e.g.* α-haloester and sacrificial electron donor) that are usually required for photoredox-mediated free radical polymerization, but concurrently needs an additional purification process to remove residues. Combined experiments and quantum chemical calculations suggest that *N*-vinyl-based monomers facilitate electron transfer between monomers and photocatalysts, which is responsible for the enhanced rate and converison of polymerization. Viscoelasticity, mechanical strength and adhesion performance of acrylic PSAs were well adjusted in a broad range by controlling the monomer composition, suggesting that our new method would replace the existing photoinitiated free radical polymerization.

Received 17th August 2020,
Accepted 23rd October 2020

DOI: 10.1039/d0gc02807j

rsc.li/greenchem

Introduction

Since the first industrial application of adhesive tape in 1874 by Johnson & Johnson, pressure-sensitive adhesives (PSAs) have been extensively utilized in various fields such as masking tapes, removable labels, decorative films, protective films, and medical tapes, which are mainly used to adhere to a variety of substrates under light pressure.[1–3] In particular, PSAs are crucial to the assembly of electronics, such as smart phones, which are essential in our daily life.[4–6]

PSAs are a special class of adhesive materials that can be classified by their chemical composition into the following categories: rubber-based, acrylic, and silicon.[1,3] Acrylic PSAs are one of the most widely used PSAs owing to their superior properties (*e.g.* resistance to oxidation, transparency, non-yellowing, and high adhesion performance).[1,3,7–9] The world market for acrylic PSAs was valued at US$ 8.84 billion in 2017 and expected to reach US$ 11.72 billion by 2022.[10] In particular, solvent-free acrylic PSA market has grown tremendously over the last few decades because (1) many governments have been enforcing more stringent regulations to control volatile organic compound emissions and (2) there can be huge possibilities to reduce the costs by eliminating the drying process and the recapturing of the evaporated solvents.[1,3,11,12]

Solvent-free acrylic PSAs are mostly prepared in the presence of photoinitiators using high-energy UV light that often raises several issues associated with the generation of ozone, radiation safety,[13,14] energy efficiency, and curing depth.[15,16] Visible-light-driven curing is thus highly required, especially for certain PSAs. For example, UV-shielding PSAs incorporate UV absorbers, and thereby, conventional UV-light curing leads to a low curing rate and monomer conversion and thus results in poor cohesion.[17,18] Visible-light curing is also necessary for

[a]*Center for Advanced Specialty Chemicals, Korea Research Institute of Chemical Technology, Ulsan 44412, Republic of Korea. E-mail: winston@krict.re.kr*
[b]*Department of Materials Science and Engineering, Seoul National University, Seoul 00826, Republic of Korea. E-mail: minsang@snu.ac.kr*
[c]*Department of Materials Science and Engineering, Ulsan National Institute of Science and Technology (UNIST), Ulsan 689-798, Republic of Korea*
[d]*Madrid Institute for Advanced Studies, IMDEA Nanoscience, Calle Faraday 9, Campus Cantoblanco, 28049 Madrid, Spain. E-mail: johhannes.gierschner@imdea.org*
[e]*Research Institute of Agriculture and Life Sciences, College of Agriculture and Life Sciences, Seoul National University, Seoul 08826, Republic of Korea*
†Electronic supplementary information (ESI) available. See DOI: 10.1039/d0gc02807j

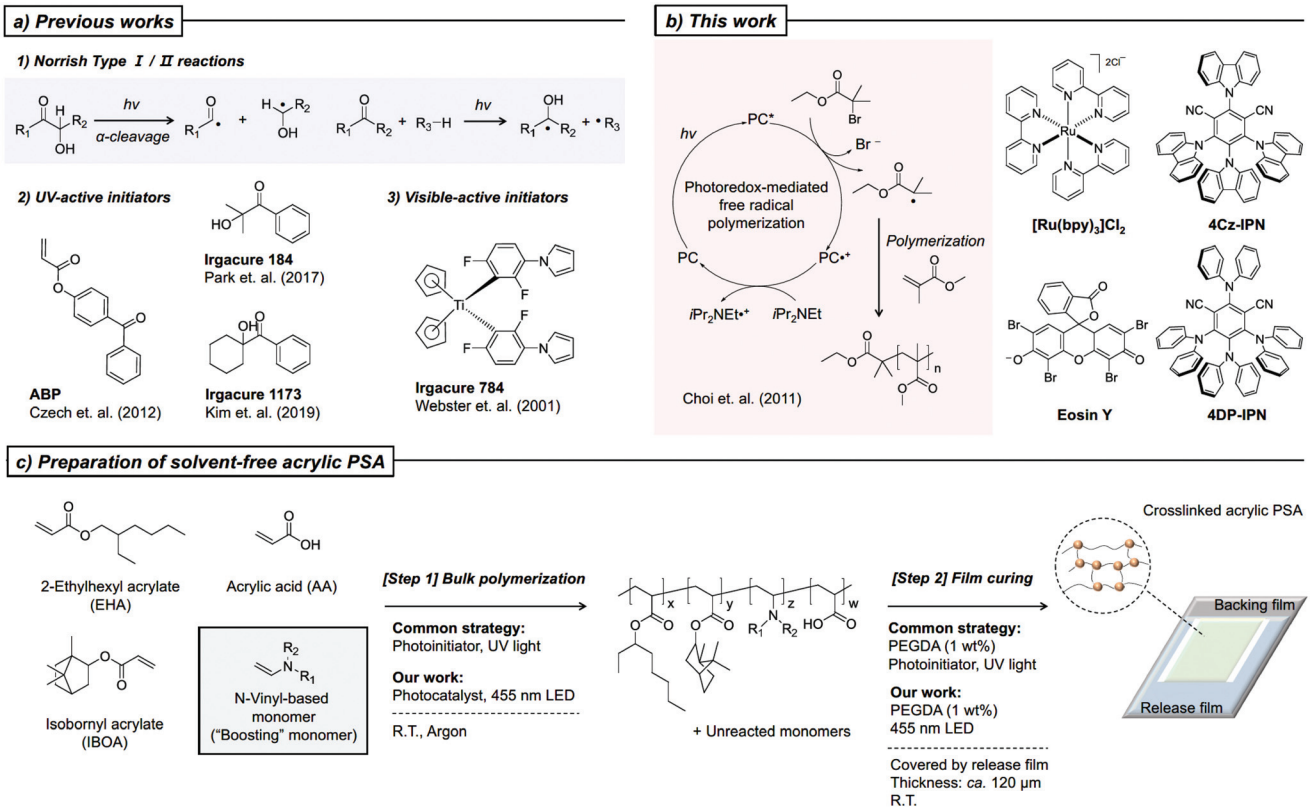

Scheme 1 (a) Conventional photoinitiators used for photocurable solvent-free acrylic PSAs and the underlying mechanism. (b) Proposed mechanism of photoredox-mediated free radical polymerization as suggested by Choi and co-workers (left) and the chemical structures of photoredox catalysts used in this study (right). (c) Schematic representation of the two-step process for the preparation of solvent-free acrylic PSAs *via* visible-light driven photoredox-mediated free radical polymerization. Network structure was formed by the crosslinking reaction of poly(ethylene glycol) diacrylate (PEGDA, M_n: 700 g mol^{-1}) and the remaining monomers.

medical PSA tapes directly attached to human skin, due to fairly harmless visible light. In spite of these advantages, only few studies on this topic have so far been reported and most of those rely on visible-light photoinitiators (Scheme 1a).[19,20]

The use of photocatalysts (PCs) has emerged as a powerful strategy in the field of photomediated polymerization.[21–25] Unlike traditional photoinitiators, PCs are regenerated in the photocatalytic cycle, and thus, only a small amount of PC is needed for the polymerization. Soft irradiation conditions such as daylight[26,27] and LED bulbs are usually required because most PCs exhibit substantial absorption of visible light. Since photocontrolled radical polymerizations based on visible-light photocatalysis were first presented,[28] a number of photocatalytic polymerizations including photoredox-mediated free radical polymerization,[28–33] photoredox-mediated atom transfer radical polymerization (ATRP),[34–39] and photoinduced electron/energy transfer reversible addition–fragmentation chain transfer (PET-RAFT) polymerization[25,40–44] have been actively developed over the last few years. Therefore, we envisaged that visible-light driven photocatalytic polymerizations could be utilized as a core strategy to prepare solvent-free acrylic PSAs (Scheme 1b).

Herein, we report a new method for the solvent-free acrylic PSAs, which does not rely on common UV photoinitiators. Instead, solvent-free acrylic PSAs were successfully prepared through photoredox-mediated free radical polymerization with a low catalyst loading of an organic photocatalyst (as low as 50 ppm; 50×10^{-6} mol% with respect to the total amount of monomers) under visible light (455 nm) LED irradiation conditions. Importantly, we found that the use of *N*-vinyl-based monomers (*N*-vinylpyrrolidone and *N*-vinylcaprolactam) largely enhances the rate and conversion of bulk polymerization and film curing, thereby eliminating the need for additives such as α-haloester and a sacrificial electron donor that are commonly used for photoredox-mediated free radical polymerization, but requires an additional purification process to remove residues. We also confirmed that the viscoelasticity, mechanical properties, and PSA performance of solvent-free PSAs were freely adjusted over a wide range, and thus, the resulting acrylic PSAs could be utilized for release coatings, general-purpose PSAs, and high-shear PSAs.

Results and discussion

Strategy

In our previous work, we discovered highly efficient organic PCs based on a systematic computer-aided-design strategy,

which addresses several issues in organocatalyzed photoredox-mediated ATRP[39] and PET-RAFT.[43] Of these, 2,4,5,6-tetrakis (diphenylamino)-1,3-benzenedicarbonitrile (4DP-IPN) was found to be one of the most efficient PCs because of (1) high visible-light absorption, (2) efficient generation of long-lived triplet excitons, (3) proper redox potentials, and (4) high photochemical and electrochemical stability, resulting in a successful control over the polymerization of methyl methacrylate (MMA) at very low catalyst loadings (0.5 ppm, 0.5×10^{-6} mol%).[39] We therefore selected 4DP-IPN as a PC for this study and also investigated 2,4,5,6-tetra-9*H*-carbazol-9-yl-1,3-benzenedicarbonitrile (4Cz-IPN) and eosin Y as a comparison for the chosen PC (Scheme 1b and Fig. S1†).

Bulk polymerization

We first investigated the photo-initiated bulk polymerization of acrylic monomers, which is the first step in the preparation of solvent-free acrylic PSAs; in fact, solvent-free acrylic PSAs are commonly prepared through the UV-induced radical photopolymerization of acrylic monomers, followed by UV-induced film curing in a sequential manner (Scheme 1c). As a control experiment, the polymerization of 2-ethylhexyl acrylate (EHA) with acrylic acid (AA) and isobornyl acrylate (IBOA) was performed in the presence of a photoinitiator of 450 ppm under an Ar atmosphere and UV irradiation conditions (Table 1, entry control). The monomer type and composition used in this polymerization is a type and composition generally utilized in the conventional solvent-free acrylic PSAs.[1] This control experiment gave poly(EHA-*co*-AA-*co*-IBOA) with a relatively good conversion (α_t = 14.4%) and high molecular weight (M_n = 664 kg mol^{-1}) only in 30 s; furthermore, it also showed an appropriate viscosity to proceed with the film curing process.

We then performed the same polymerization with 4DP-IPN of 50 ppm (instead of the photoinitiator) under an Ar atmosphere and 455 nm LED irradiation conditions (Table 1, entry 2). Poly(EHA-*co*-AA-*co*-IBOA) was obtained with a rather good conversion (α_t = 9.9%) and molecular weight (M_n = 948 kg mol^{-1}) and thus proper viscosity, but in a much longer time of 280 s. We attributed this slow reaction rate to an inefficient initiation process that probably originates from the absence of α-haloester and sacrificial electron donors such as *N*,*N*-diisopropylethylamine (DIPEA), which is commonly required to undergo photoredox-mediated free radical polymerization.[28,45,46] In fact, the addition of diethyl 2-bromo-2-methylmalonate (DBM) considerably enhanced the rate of polymerization (Table 1, entry 3); however, this may require additional purification processes to remove residues and/or contaminants from the additives.

According to several recent studies, the rate of polymerization and the final conversion are substantially increased in photomediated radical polymerizations by the addition of *N*-vinylpyrrolidone (NVP) as a comonomer.[30,47,48] Several hypotheses have been proposed to explain such a rate enhancement; however, the conclusion remains somewhat controversial.[30,47,48] We therefore incorporated NVP as a comonomer to increase the rate of bulk polymerization. Here, the total amount of high T_g monomers (*i.e.* IBOA and NVP) was

Table 1 Results of the bulk polymerization. Negative control (entries control and 1), different amounts of *N*-vinylpyrrolidone (NVP, entries 2 and 5–8), additive (diethyl 2-bromo-2-methylmalonate = DBM, entry 3), different PC amounts (entries 6, 11, and 12) and different types of *N*-vinyl monomers (entry 13) were employed. Total conversion of bulk polymerization (α_t) was characterized by ^{1}H-NMR (see Fig. S10†). Number average molecular weight (M_n) was characterized by size exclusion chromatography (SEC). *Đ* represents dispersity

Entry	Additive	[IBOA] : [NVP] : [PC][a]	Time (s)	α_t (%)	M_n (kg mol^{-1})	*Đ*
Control[b]	—	30 : 0 : 0.045	30	14.4	665	1.77
1	—	30 : 0 : 0	>4200	0	—	—
2	—	30 : 0 : 0.005	280	9.9	948	1.52
3	DBM	30 : 0 : 0.005	12	12.5	278	2.28
4	—	20 : 10 : 0	>4200	0	—	—
5	—	25 : 5 : 0.005	220	11.3	709	1.74
6	—	20 : 10 : 0.005	145	10.6	655	1.64
7	—	10 : 20 : 0.005	90	10.9	353	1.82
8	—	0 : 30 : 0.005	60	13.4	143	2.32
9[c]	—	0 : 30 : 0.005	720	0	—	—
10[d]	—	0 : 30 : 0.005	60	3.9	394	2.11
11	—	20 : 10 : 0.0005	520	9.5	510	1.65
12	—	20 : 10 : 0.05	1160	12.9	688	1.84
13[e]	—	20 : 10 : 0.005	170	9.1	560	1.81

[a] [EHA] : [AA] = 65 : 5 (*e.g.* for entry 6 in Table 1, [EHA] : [AA] : [IBOA] : [NVP] : [PC] was set as 65 : 5 : 20 : 10 : 0.005). 4DP-IPN was used as a photocatalyst (PC). [b] Photoinitiator was used instead of a photocatalyst. Polymerization was performed. [c] Without argon bubbling. [d] In the presence of 0.3 wt% of MEHQ. [e] *N*-Vinylcaprolactam (NVC) was used instead of NVP.

fixed at 30 mol% to minimize the change in T_g of the resulting PSAs.

Table 1 shows the results of the bulk polymerization in the presence of NVP; the optimal catalyst loading was found to be 50 ppm (Table 1, entries 6, 11, and 12). As expected, the rate of polymerization was considerably enhanced as the amount of NVP increased (Table 1, entries 2 and 5–8). Interestingly, an increase in the amount of NVP resulted in a significant decrease in the number average molecular weight (M_n), indicating that NVP might act as an initiator as well as a monomer of photomediated polymerization. However, considering both the NVP content and the resulting M_n, only a small amount of NVP might be involved in the initiation process.

Polymerization mechanism

According to (time-dependent) density functional theory, (TD) DFT, calculations as shown in Fig. 1a and Fig. S2,† the initiation process most likely proceeds through the electron transfer from NVP to 4DP-IPN in the excited state. Considering the lowest singlet/triplet state (S_1/T_1) energies of 4DP-IPN, NVP, and methyl acrylate (MA), the initiation does not appear to occur through the energy transfer pathway (Fig. S2†). In fact, the highest occupied molecular orbital (HOMO) energy of NVP is 1.56 eV, higher than that of MA, which results in a relatively faster electron transfer from the HOMO of NVP to the lowest singly occupied molecular orbital (SOMO) of 4DP-IPN in S_1 and/or T_1 as compared to that between MA and the S_1/T_1 of 4DP-IPN (Fig. 1c). Moreover, the calculated MO diagrams of 4DP-IPN and NVP show that the photoinduced electron transfer (PeT) from NVP to 4DP-IPN should be endothermic. Hence, only a very small amount of NVP is expected to participate in the initiation process, which is in accordance with the experimental results. Our hypothesis is also supported by the fact that the singlet and triplet excited state reduction potentials (E^*_{red}) of 4DP-IPN are 0.93 V and 0.76 V, respectively,[39] which are similar to the voltage of *ca.* 1.1 V at which the electrochemical polymerization of NVP starts to occur.[49] A similar rate enhancement was also observed for the structurally similar monomer of *N*-vinylcaprolactam (NVC), implying that *N*-vinyl monomers might be used as an initiator as well as a monomer for photomediated polymerizations (Table 1, entry 13).

The polymerization mechanism was further investigated in detail. In Table 1, entries 9 and 10 show the results of polymerizations carried out in the presence of oxygen and a radical stabilizer (*i.e.* 4-methoxyphenol (MEHQ)), respectively. Inhibition or significant retardation was observed in each polymerization reaction, implying that the polymerization obviously proceeds *via* a radical mechanism. In order to reveal the radical intermediate involved in the initiation step, DFT calculations were performed for the relative energies of NVP radical cation (NVP$^{\bullet}$+) and its possible tautomers produced by endothermic PeT. Based on the DFT results, it is observed that *tc*-NVP$^{\bullet}$+ (one contributing resonance form of NVP$^{\bullet}$+) can be the most plausible candidate (Fig. 1d) since (1) it has significantly lower energies compared to other tautomers (Fig. 1g) and, concurrently, (2) it has a radical character at the C_{v2} carbon atom, resulting in sufficient reactivity to an acrylic monomer. This can be seen from the molecular orbital (MO) analysis, which confirms a significant weight of the *tc*-NVP$^{\bullet}$+ resonance structure to NVP$^{\bullet}$+. Neutral NVP shows a bonding character between N and C_O (see Fig. 1e), indicating that the zwitterionic resonance structure (N^+, O^-; see *z*-NVP in Fig. 1d) has a relatively high weight *vs.* the neutral one. This is confirmed by the rather short N–C_O bond length (1.38 Å). On the other hand, the CN bond with vinylene C is relatively long with N–C_{V1} = 1.39 Å, while C_{V1}–C_{V2} = 1.34 Å is short. In NVP$^{\bullet}$+, the electron density at the N–C_O bond is reduced (Fig. 1f), so that N–C_O is long (1.49 Å), while N–C_{V1} is short (1.33 Å), and C_{V1}–C_{V2} is elongated (1.39 Å), indeed suggesting a partial radical character at C_{V2}.

Initiation can be reasonably predicted from the combined experiments and DFT calculations, whereas the catalyst regeneration process is still largely unclear although several pathways are shown in Fig. 1d. However, it should be noted that catalyst regeneration certainly exists because it was clearly observed that the catalysts were almost preserved before and after the bulk polymerization (Fig. S3†). We are currently performing further mechanistic investigations for the catalyst regeneration.

Curing of prepolymer mixture

We then investigated the visible-light curing process of the prepolymer mixture obtained above. Here, a small amount of the cross-linker (*i.e.* poly(ethylene glycol) diacrylate, PEGDA, M_n: 700 g mol^{-1}, 1 wt%) was further included in the prepolymer mixture for the curing process (Scheme 1c). Unlike the conventional UV-curing process, additional photoinitiators and/or photocatalysts were not required because the photocatalysts may not be consumed in the bulk polymerization; in fact, they mostly remain in the prepolymer mixture (Fig. S3†). The resulting mixture was coated onto a backing film (polyethylene terephthalate film, 50 μm), and then a release film was subsequently covered on the surface; the final thickness of the film was set to *ca.* 120 μm. A string type LED (448 nm, 0.3 mW cm^{-2}, three strings) was employed for film curing.

The monomer conversion at the film (α_f) as a function of curing time is shown in Fig. 2a; the conversion is determined by using Fourier-transform infrared spectroscopy (FTIR) measurements in ATR mode by which the time evolution of the C=C bending peak at 830–795 cm^{-1} and the C=O stretching peak at 1760–1660 cm^{-1} are recorded as a function of the wavenumber (Fig. 2b). Without additional photocatalysts and/or photoinitiators, film curing successfully occurred as expected and a significant increase in the cure rate was also observed in the presence of NVP, which is the same phenomenon observed in bulk polymerization (Fig. 2a). Despite this rate enhancement, the cure rate is still far below the rate observed in the conventional UV curing system (Fig. S4a†). We attributed this mainly to the low power density of the light source (Fig. S4†); a highly reliable high-power-density light source is currently being setup.

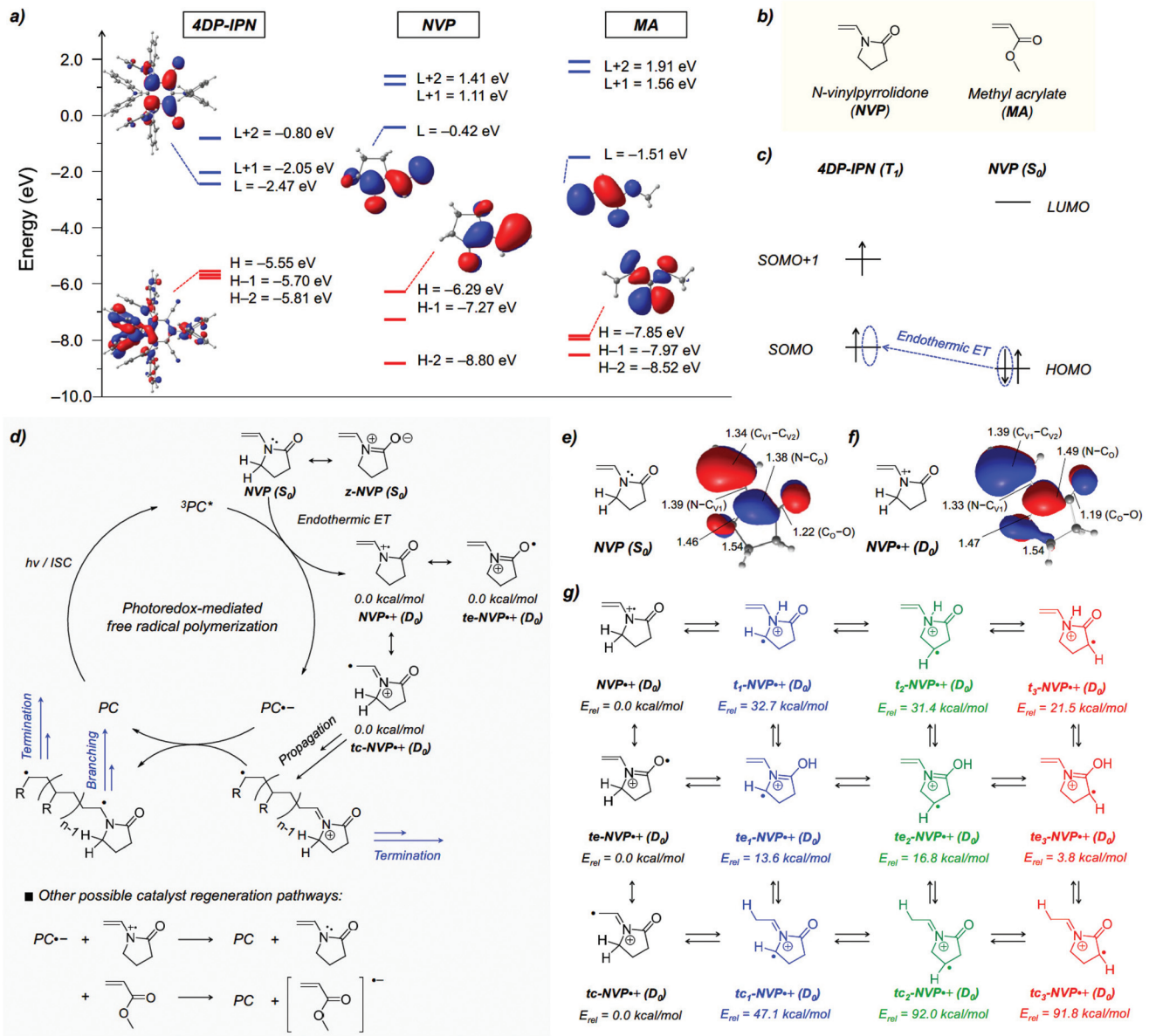

Fig. 1 (a) DFT calculated MO diagram of 4DP-IPN (left), NVP (middle), and MA (right). Calculated HOMO and LUMO topologies of 4DP-IPN, NVP, and MA are also shown. (b) Chemical structures of NVP (left) and MA (right) are shown. (c) Schematic diagram for the endothermic electron transfer from NVP (S_0) to 4DP-IPN (T_1). (d) Proposed mechanism of additive-free photoredox-mediated free radical polymerization. MO topologies of (e) NVP (S_0) and (f) NVP$^{\bullet+}$ (D_0) are shown with their chemical structure and bond length. (g) Relative energies of NVP and its possible tautomers calculated by DFT are shown.

Viscoelastic properties of the cured films

It is essential to characterize the viscoelastic properties of PSAs because the tack, peel, and shear strength of PSAs greatly rely on their viscoelastic properties.[1,50] According to Chang, viscoelastic windows can be constructed by the measurement of dynamic storage modulus (G') and dynamic loss modulus (G'') at the application frequencies and temperature, which identify the potential applications of PSAs (Fig. 3a).[50] Therefore, we investigated the viscoelastic properties of the PSAs prepared using our strategy and constructed the viscoelastic windows. Viscoelasticity of the laminated PSA (thickness: 0.8 mm) was characterized by dynamic mechanical analysis (DMA) with a shear sandwich clamp (frequency: 0.01–100 Hz, temperature: 23 °C, strain: 1%, see the ESI† for details).

Six different PSAs were first designed by considering certain factors (*e.g.* glass transition temperature (T_g) and polar monomer contents), which are known to affect the viscoelastic properties of PSAs (Table 2). We then prepared six different prepolymer mixtures in a series of bulk polymerizations with fixed PEGDA and NVP contents (1 wt% and 10 mol%) and varying amounts of EHA, AA, and IBOA. It should be noted that NVP was fixed at

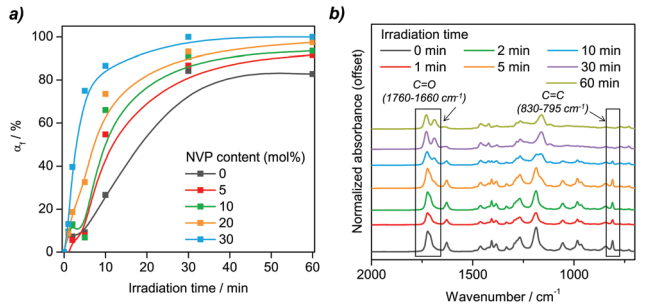

Fig. 2 (a) The film conversion (α_f) is plotted as a function of curing time for different NVP contents (entries 2 and 5–8 in Table 1), and (b) FT-IR spectra over irradiation time are shown (entry 6 in Table 1).

10 mol% to enhance the rate and final conversion of both bulk polymerization and film curing. Although NVP was incorporated as a boosting monomer, the polymerization rate was still slow in certain compositions (Table 2, entry 6), which implies the necessity of further research on the mechanism of photoredox-mediated free radical polymerization.

Storage modulus increased as the amount of high T_g monomer (*e.g.*, IBOA and NVP) increased, as expected (Fig. 3b and Fig. S5a†). As shown in Fig. 3c, the prepared PSAs did not cover the region 3 and 4, which are usually covered by other types of PSAs, *e.g.* silicone PSAs.[50] Although the prepared PSAs could not cover the region 3 and 4 due to its intrinsic material's limitation, storage modulus of acrylic PSAs could be controlled in a quite wide range, which mostly covers the region 1, 2, and 5. It thus suggests that the prepared PSAs can be utilized in most applications such as release coatings, general-purpose PSAs, and high-shear PSAs where conventional acrylic PSAs are used.[8,50]

Mechanical and PSA properties of the cured films

Finally, we investigated the mechanical and adhesive properties, film conversion, and gel fraction of the prepared PSAs (Table 3). Film curing for all compositions was successful as indicated by the high film conversion (>86%), and the gel fraction varied from 88.3% to 95.0%.

Single lap shear tests were conducted to obtain the strain–stress curves by using a universal testing machine (UTM) with a constant cross-head speed (1 mm s^{-1}, see the ESI† for details). As shown in Fig. 3d and Table 3, both the lap shear strength and elongation at breaks generally increased as the amount of high T_g monomer (*e.g.*, IBOA and NVP) increased, which implies that the toughness of PSAs can be easily adjusted by the monomer composition. The lap shear strengths of the prepared PSAs (0.189–0.254 MPa) correspond well with those of the previously reported photoresponsive acrylic adhesives (0.150–0.341 MPa).[51,52]

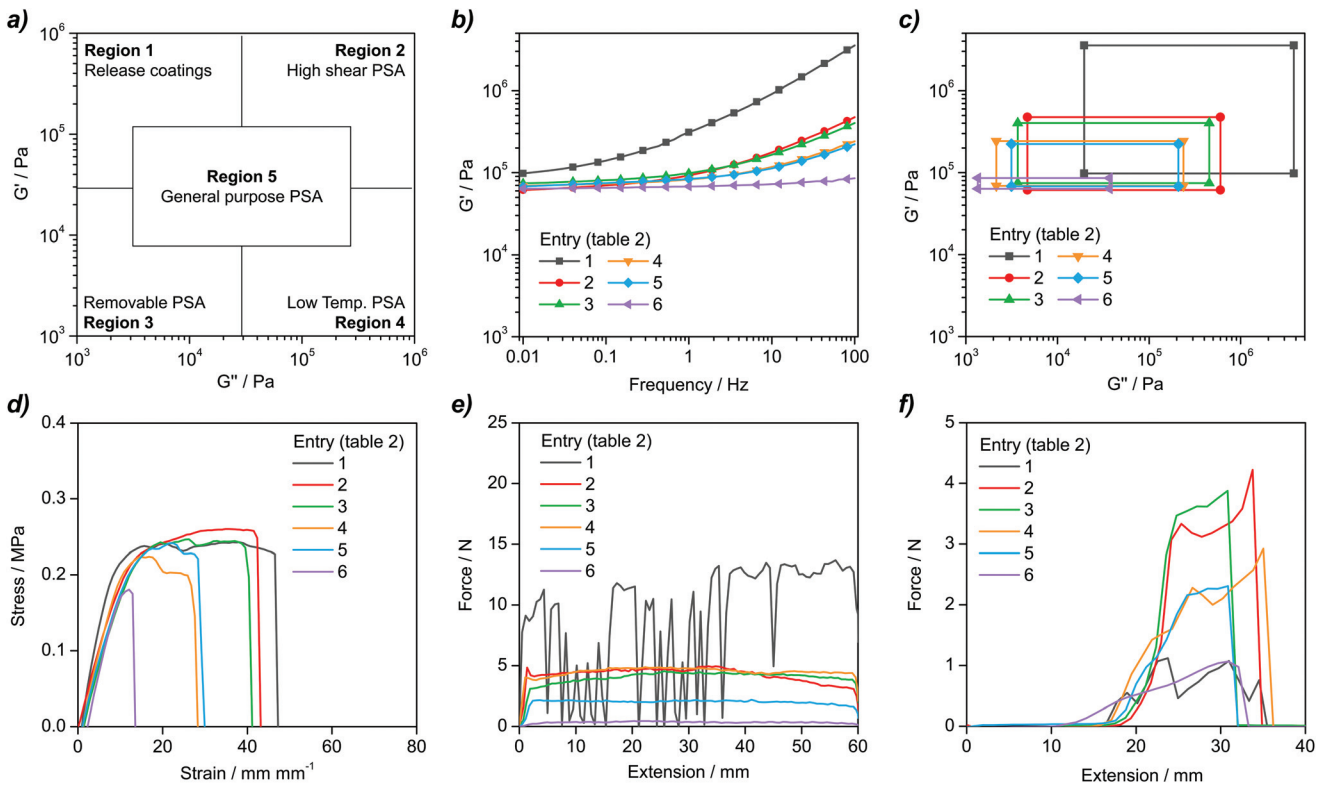

Fig. 3 (a) Viscoelastic window of PSAs and the proposed application area according to each region.[50] (b) Frequency–storage modulus curve and (c) the viscoelastic window of various PSAs (entries 1–6 in Table 2). (d) Strain–stress curve of lap shear test, (e) the extension–force curve from the 180° peel test (substrate: stainless steel), and (f) the extension–force curve from the loop tack test of various PSAs (substrate: stainless steel, entries 1–6 in Table 2). The irradiation time of blue LED for film curing was set as 60 min for all PSAs.

Table 2 Results of the bulk polymerization for the preparation of solvent-free acrylic PSAs with different monomer compositions; $T_{g,cal}$ was the expected glass transition temperature calculated by the Flory–Fox equation. $T_{g,exp}$ was the experimental glass transition temperature of the cured film and was characterized by differential scanning calorimetry (see Fig. S7†)

Entry	[EHA] : [AA] : [IBOA][a]	$T_{g,cal}$ (°C)	$T_{g,exp}$ (°C)	Time (s)	α_t (%)	M_n (kg mol^{-1})	$Đ$
1	50 : 10 : 30	−17.6	−22.3	170	11.60	156	3.23
2	50 : 5 : 35	−12.1	−30.3	130	11.65	336	1.95
3	60 : 5 : 25	−30.1	−34.4	115	9.11	512	1.78
4	70 : 5 : 15	−44.0	−42.2	130	10.12	740	1.72
5	80 : 5 : 5	−56.8	−49.7	115	8.68	573	1.69
6	90 : 0 : 0	−65.0	— (not observed)	1273	9.44	1075	1.61

[a] [NVP] : [PC] = 10 : 0.005.

Table 3 Lap shear strength, elongation at break, peel strength, loop tack, gel fraction and film conversion of various PSAs (entries 1–6 in Table 2). The characterization methods were detailed in the ESI.† The irradiation time of blue LED for film curing was set as 60 min for all PSAs

			Peel strength (N cm^{-1})		Loop tack (N cm^{-1})			
Entry (Table 2)	Lap shear strength (MPa)	Elongation at break (mm mm^{-1})	Stainless steel	Glass	Stainless steel	Glass	Film conversion (α_f, %)	Gel fraction (%)
1	0.242 (±0.007)	47.50 (±5.64)	9.90[a] (±1.12)	5.87 (±0.34)	1.15 (±0.30)	5.59 (±0.45)	90.6	90.8
2	0.254 (±0.013)	42.36 (±2.25)	4.51 (±0.31)	4.73 (±0.16)	4.59 (±0.69)	7.51 (±0.57)	86.3	88.8
3	0.246 (±0.007)	37.89 (±3.55)	4.17 (±0.37)	3.52 (±0.24)	5.15 (±0.57)	7.63 (±0.44)	90.3	92.4
4	0.224 (±0.003)	26.71 (±2.79)	4.59 (±0.16)	2.56 (±0.11)	3.35 (±0.18)	4.39 (±0.47)	90.8	88.3
5	0.228 (±0.009)	28.34 (±3.03)	2.05 (±0.15)	1.59 (±0.09)	3.38 (±0.36)	4.56 (±0.43)	94.4	95.0
6	0.189 (±0.014)	13.62 (±0.98)	0.40 (±0.08)	0.26 (±0.04)	1.98 (±0.28)	2.17 (±0.59)	93.3	93.2

[a] Stick-slip was observed in a debonding experiment.

The PSA properties of the prepared PSA films were assessed by a 180° peel and loop tack test with different types of substrates (stainless steel and glass), using a 50 μm thick polyethylene terephthalate as a backing film (Fig. 3e, f, and Table 3, see the ESI† for details). The loop tack was higher for a glass substrate as compared to stainless steel, since PSAs show a better wettability for a glass with a higher surface energy and lower roughness than stainless steel.[53] In contrast, the peel strength was higher in stainless steel, which may originate from superior mechanical interlocking between PSAs and rough surface of stainless steel. For the PSAs listed in Table 3, entry 1, despite its superior peel strength, loop tack value was inferior and stick-slip was observed in a debonding experiment (Fig. 3e, dark grey line), which is normally observed in glassy polymers. Conclusively, optimal peel strength (4.17–4.59 N cm^{-1}, stainless steel) and loop tack (3.35–4.59 N cm^{-1}, stainless steel) were found in most compositions (entries 2–4), which are comparable to commercially available PSAs, for example, duct tape (peel strength: 4 N cm^{-1}; tack: 5 N cm^{-1}).[54,55] These results further confirmed that our strategy can be broadly applied to prepare solvent-free acrylic PSAs for a variety of applications.

Conclusions

In summary, for the first time, solvent-free acrylic PSAs were fabricated *via* an organocatalyzed photoredox-mediated free radical polymerization. Both bulk polymerization and film curing proceeded smoothly in the presence of a small amount of an organic photocatalyst under visible-light irradiation conditions. Combined experimental and quantum chemical studies revealed that *N*-vinyl monomers greatly enhanced the rate and monomer conversion of both bulk polymerization and film curing, resulting in the successful preparation of solvent-free acrylic PSAs without any additives under extremely mild conditions. Through investigations of viscoelastic, mechanical, and adhesive properties of the PSAs prepared by the developed method, we clearly confirmed that our method can be broadly applied to prepare solvent-free acrylic PSAs for a variety of applications. Therefore, we believe that our work might address a variety of challenging tasks related to solvent-free acrylic PSAs, particularly for UV-shielding PSAs and medical PSA tapes.

Conflicts of interest

There are no conflicts to declare.

Acknowledgements

The work at SNU was supported by the Technology Innovation Program (20010768, Development of Fast Curing Structural Adhesive with High Performance for Dissimilar Materials on High Speed Process) funded by the Ministry of Trade, Industry

and Energy and by the Institute of Civil Military Technology Cooperation Center (ICMTC) funded by the Ministry of Trade, Industry and Energy, and Defense Acquisition Program Administration of Korea (18-CM-SS13). The work at KRICT was supported by the Korea Research Institute of Chemical Technology (grant number SS2041-10). The work in Madrid was supported by the MINECO-FEDER project CTQ2017-87054, by the "Severo Ochoa" program for Centers of Excellence in R&D of the MINECO (SEV-2016-0686) and by the Campus of International Excellence (CEI) UAM + CSIC.

Notes and references

1 D. Satas, *Handbook of pressure sensitive adhesive technology*, Satas & Associates, Warwick, 3rd edn, 1999.
2 E. E. Dickson, *US Pat.*, 1612267A, 1926.
3 C. Creton, *MRS Bull.*, 2003, **28**, 434–439.
4 Y. Li, K.-s. Moon and C. Wong, *Science*, 2005, **308**, 1419–1420.
5 C. Murray, R. Rudman, M. Sabade and A. Pocius, *MRS Bull.*, 2003, **28**, 449–454.
6 Smartphones market - Growth, trends, and forecast (2020–2025), Mordor Intelligence LLP, Tlangana, 2020.
7 S. D. Tobing and A. Klein, *J. Appl. Polym. Sci.*, 2001, **79**, 2230–2244.
8 J. J. Gallagher, M. A. Hillmyer and T. M. Reineke, *ACS Sustainable Chem. Eng.*, 2016, **4**, 3379–3387.
9 M. Nasiri, D. J. Saxon and T. M. Reineke, *Macromolecules*, 2018, **51**, 2456–2465.
10 Acrylic Adhesives Market by Type (Acrylic Polymer Emulsion, Cyanoacrylic, Methacrylic, UV Curable Acrylic), Application (Paper & Packaging, Construction, Transportation, Medical, Consumer, Electronics), Technology, and Region - Global Forecast to 2022, Markets and Markets, Maharashtra, 2017.
11 H. Moon, K. Jeong, M. J. Kwak, S. Q. Choi and S. G. Im, *ACS Appl. Mater. Interfaces*, 2018, **10**, 32668–32677.
12 Z. Czech and R. Milker, *J. Appl. Polym. Sci.*, 2003, **87**, 182–191.
13 M. Ichihashi, M. Ueda, A. Budiyanto, T. Bito, M. Oka, M. Fukunaga, K. Tsuru and T. Horikawa, *Toxicology*, 2003, **189**, 21–39.
14 G. J. Clydesdale, G. W. Dandie and H. K. Muller, *Immunol. Cell Biol.*, 2001, **79**, 547–568.
15 J. Hu, Y. Hou, H. Park, B. Choi, S. Hou, A. Chung and M. Lee, *Acta Biomater.*, 2012, **8**, 1730–1738.
16 J. Elisseeff, K. Anseth, D. Sims, W. McIntosh, M. Randolph and R. Langer, *Proc. Natl. Acad. Sci. U. S. A.*, 1999, **96**, 3104–3107.
17 J. Yokoyama, Y. Soeda, Y. Tosaki and K. Ikeda, *US Pat.*, 8673443B2, 2014.
18 Y. Yin, S. Zhou, G. Gu and L. Wu, *J. Mater. Sci.*, 2007, **42**, 5959–5963.
19 I. Webster, *Int. J. Adhes. Adhes.*, 1999, **19**, 29–34.
20 J. Boyne, E. Millan and I. Webster, *Int. J. Adhes. Adhes.*, 2001, **21**, 49–53.
21 Y. Lee and M. S. Kwon, Emerging organic photoredox catalysts for organic transformations, *Eur. J. Org. Chem.*, 2020, **38**, 6028–6043.
22 M. Chen, M. Zhong and J. A. Johnson, *Chem. Rev.*, 2016, **116**, 10167–10211.
23 N. Corrigan, S. Shanmugam, J. Xu and C. Boyer, *Chem. Soc. Rev.*, 2016, **45**, 6165–6212.
24 X. Pan, M. A. Tasdelen, J. Laun, T. Junkers, Y. Yagci and K. Matyjaszewski, *Prog. Polym. Sci.*, 2016, **62**, 73–125.
25 T. G. McKenzie, Q. Fu, M. Uchiyama, K. Satoh, J. Xu, C. Boyer, M. Kamigaito and G. G. Qiao, *Adv. Sci.*, 2016, **3**, 1500394.
26 J. Jiang, G. Ye, Z. Wang, Y. Lu, J. Chen and K. Matyjaszewski, *Angew. Chem., Int. Ed.*, 2018, **57**, 12037–12042.
27 M.-A. Tehfe, J. Lalevee, D. Gigmes and J. P. Fouassier, *Macromolecules*, 2010, **43**, 1364–1370.
28 G. Zhang, I. Y. Song, K. H. Ahn, T. Park and W. Choi, *Macromolecules*, 2011, **44**, 7594–7599.
29 Y. Yagci, M. Sangermano and G. Rizza, *Chem. Commun.*, 2008, 2771–2773.
30 A. Aguirre-Soto, S. Kim, K. Kaastrup and H. D. Sikes, *Polym. Chem.*, 2019, **10**, 926–937.
31 P. Xiao, J. Zhang, F. Dumur, M. A. Tehfe, F. Morlet-Savary, B. Graff, D. Gigmes, J. P. Fouassier and J. Lalevee, *Prog. Polym. Sci.*, 2015, **41**, 32–66.
32 J. Lalevée, M.-A. Tehfe, F. Dumur, D. Gigmes, N. Blanchard, F. Morlet-Savary and J. P. Fouassier, *ACS Macro Lett.*, 2012, **1**, 286–290.
33 M.-A. Tehfe, J. Lalevée, F. Morlet-Savary, B. Graff, N. Blanchard and J.-P. Fouassier, *Macromolecules*, 2012, **45**, 1746–1752.
34 B. P. Fors and C. J. Hawker, *Angew. Chem., Int. Ed.*, 2012, **51**, 8850–8853.
35 J. C. Theriot, C.-H. Lim, H. Yang, M. D. Ryan, C. B. Musgrave and G. M. Miyake, *Science*, 2016, **352**, 1082–1086.
36 R. M. Pearson, C.-H. Lim, B. G. McCarthy, C. B. Musgrave and G. M. Miyake, *J. Am. Chem. Soc.*, 2016, **138**, 11399–11407.
37 X. Pan, C. Fang, M. Fantin, N. Malhotra, W. Y. So, L. A. Peteanu, A. A. Isse, A. Gennaro, P. Liu and K. Matyjaszewski, *J. Am. Chem. Soc.*, 2016, **138**, 2411–2425.
38 C.-H. Lim, M. D. Ryan, B. G. McCarthy, J. C. Theriot, S. M. Sartor, N. H. Damrauer, C. B. Musgrave and G. M. Miyake, *J. Am. Chem. Soc.*, 2017, **139**, 348–355.
39 V. K. Singh, C. Yu, S. Badgujar, Y. Kim, Y. Kwon, D. Kim, J. Lee, T. Akhter, G. Thangavel, L. S. Park, J. Lee, P. C. Nandajan, R. Wannemacher, B. Milián-Medina, L. Lüer, K. S. Kim, J. Gierschner and M. S. Kwon, *Nat. Catal.*, 2018, **1**, 794–804.
40 J. Xu, K. Jung, A. Atme, S. Shanmugam and C. Boyer, *J. Am. Chem. Soc.*, 2014, **136**, 5508–5519.

41 M. Chen, M. J. MacLeod and J. A. Johnson, *ACS Macro Lett.*, 2015, **4**, 566–569.
42 Q. Fu, K. Xie, T. McKenzie and G. Qiao, *Polym. Chem.*, 2017, **8**, 1519–1526.
43 Y. Song, Y. Kim, Y. Noh, V. K. Singh, S. K. Behera, A. Abudulimu, K. Chung, R. Wannemacher, J. Gierschner, L. Lüer and M. S. Kwon, *Macromolecules*, 2019, **52**, 5538–5545.
44 J. Phommalysack-Lovan, Y. Chu, C. Boyer and J. Xu, *Chem. Commun.*, 2018, **54**, 6591–6606.
45 B. Nomeir, O. Fabre and K. Ferji, *Macromolecules*, 2019, **52**, 6898–6903.
46 S. Kızılel, V. H. Pérez-Luna and F. Teymour, *Langmuir*, 2004, **20**, 8652–8658.
47 T. J. White, W. B. Liechty and C. A. Guymon, *J. Polym. Sci., Part A: Polym. Chem.*, 2007, **45**, 4062–4073.
48 T. J. White, W. B. Liechty, L. V. Natarajan, V. P. Tondiglia, T. J. Bunning and C. A. Guymon, *Polymer*, 2006, **47**, 2289–2298.
49 C. Doneux, R. Caudano, J. Delhalle, E. Leonard-Stibbe, J. Charlier, C. Bureau, J. Tanguy and G. Lécayon, *Langmuir*, 1997, **13**, 4898–4905.
50 E. Chang, *J. Adhes.*, 1991, **34**, 189–200.
51 T. Harper, R. Slegeris, I. Pramudya and H. Chung, *ACS Appl. Mater. Interfaces*, 2017, **9**, 1830–1839.
52 M. Kim and H. Chung, *Polym. Chem.*, 2017, **8**, 6300–6308.
53 A. Kowalski and Z. Czech, *Int. J. Adhes. Adhes.*, 2015, **60**, 9–15.
54 G. S. Sulley, G. L. Gregory, T. T. D. Chen, L. P. Carrodeguas, G. Trott, A. Santmarti, K.-Y. Lee, N. J. Terrill and C. K. Williams, *J. Am. Chem. Soc.*, 2020, **142**, 4367–4378.
55 A. Beharaj, I. Ekladious and M. W. Grinstaff, *Angew. Chem., Int. Ed.*, 2019, **58**, 1407–1411.